Aeroelastic Load Analysis of a Co-Rotating Quad-Rotor Wind Turbine

Etana Ferede[1] and Farhan Gandhi[2]

Center for Mobility with Vertical Lift (MOVE)
Rensselaer Polytechnic Institute, Troy, NY, 12180, USA

A quad-rotor wind turbine with combined rated power of 6MW and a single-rotor with equivalent machine rating are modelled in SIMAPCK coupled with AerodynV15 (including turbulent wind input from TurbSim) to calculate the aerodynamic loads on the rotors. A correction for tower/boom shadow is implemented in Matlab to account for reduction in (axial) incoming wind due to the presence of support structures that carry the rotors. The performance of the quad-rotor wind turbine, with the single-rotor as baseline, is carried out for load cases selected from wind turbine certification standard (IEC-61400-1) covering: nominal loads under normal wind speed profile, fatigue loads under normal turbulence, and ultimate loads under extreme turbulence. Results show that, comparing the quad-rotor tower root loads to those of the single-rotor turbine under extreme turbulence, the side-side force is up to 31% higher, the force-aft bending moment is up to 15% higher, and the normal force is up to 46% higher due to additional boom/nacelle inertial loads.

I. Introduction

A key metric in the wind energy industry is the Cost of Energy (COE) which is critical in evaluating electricity generated from wind compared to other sources. This has led both the scientific community and the industry to continuously search for approaches to reduce the COE in order to make it competitive with already established methods for generating electricity. One way of reducing the COE is by increasing the Annual Energy Production (AEP). AEP is increased by expanding the rotor swept area in order to maximize energy capture from wind. As a result, the trend in wind energy industry is towards larger wind turbines, especially for offshore wind farms. Unfortunately, scaling of the existing wind turbine components increases the COE since AEP is proportional to the square of rotor radius while the cost of wind turbine components is proportional to the cubic of rotor radius, occasionally referred to as the square-cube law in the wind energy community. An alternative to the square-cube law is the Multi-Rotor concept, where two or more rotors are placed on a single tower.

Multi-Rotor wind turbines are not a new concept. The concept dates back to the early 19th century, where a Danish wind mill is modified to a twin-rotor wind mill [1]. The first Multi-Rotor wind turbine concept for generating electric power is proposed in 1932 [2]. The Dutch company Lagerwey, in the late 20th century, built and operated several Multi-Rotor wind turbines [3]. The proposed concepts are comprised of two, four and six two-bladed rotors on a single tower. NASA Langley wind tunnel in Virginia tested in 2010 seven rotors supported on a hexagonal frame [3]; concluding that no significant power loss is observed for lateral spacing between rotors as close as 5% of rotor diameter, agreeing with the finding from similar wind tunnel experiment in 1984 [4]. Recently in 2016, Vestas Wind Energy Systems A/S constructed and tested four three-bladed V29-225KW rotors on a single tower [6]. The experiment lasted for about three years and decommissioned in late 2018, concluding faster wake recovery compared to a single-rotor wind turbine with equivalent rotor area and thus having the potential of reducing turbine spacing in a wind farm composed (at least in part) of Multi-Rotor wind turbines.

Great progress is made with regards to the aerodynamic performance of Multi-Rotor wind turbines. Several aerodynamic research endeavors on Multi-Rotor wind turbines have shown an increase in energy extraction compared to a Single-Rotor wind turbine with equal swept area [7,8]. The distance between rotors on a Multi-Rotor wind turbine influences the aerodynamic interaction of the rotors [7,9]. Furthermore, it is observed that closely spacing the rotors on a Multi-Rotor wind turbine increases the loading on the blades which requires a further examination by means of

[1] Research Scientist, Center for Mobility with Vertical Lift (MOVE), ferede@rpi.edu.
[2] Redfern Chair Professor and MOVE Director, AIAA Fellow, fgandhi@rpi.edu.

aeroelastic simulation of a Multi-Rotor wind turbine [7]. An aerodynamic analysis of a Multi-Rotor wind turbine comprised of four rotors indicate faster wake recovery as well as reduced Turbulence Kinetic Energy (TKE) compared to a Single-Rotor wind turbine with equal swept area [10–13]. The reduction of TKE in Multi-Rotor wind turbine wake has the potential of reduced fatigue loads on the downstream wind turbines in a wind farm.

Multi-Rotor wind turbines can potentially retain the economic advantage of smaller scale systems while achieving the power gain of larger Single-Rotor wind turbines with equivalent swept area. The ratio of the (rotor) mass of Multi-Rotor turbine to that of a Single-Rotor system with equal swept area is $\frac{1}{\sqrt{n}}$, where n is the number or rotors on the Multi-Rotor system [5]. This ratio indicates that the rotor mass of a Multi-Rotor wind turbine decreases with increased number of rotors, compared to a Single-Rotor wind turbine with equal swept area. However, it does not account for the added mass of the support structure (booms that support the individual rotors and attach to the main tower) and possible mass increase of the tower as a consequence of altered loading compared to a tower with a large Single-Rotor. A structural analysis is carried out for a Multi-Rotor wind turbine consisting of $45 \times 444 KW$ rotors on a single tower, designed for offshore environment [9, 14]. The design considered pertinent loads cases from IEC-61400-1 [15]. The findings suggest that the benefit in COE reduction for Multi-Rotor turbine due to reduced rotor and drive train cost will not be significantly affected by the increased cost of the support structure on a Multi-Rotor system. Furthermore, Multi-Rotor wind turbines have additional advantage over Single-Rotor wind turbine, such as quicker response time of the smaller rotors to variation in wind speed and standardization of components that increases the reliability and thus drives down the cost of energy. However, the model used in [9, 14] does not account for the aeroelastic effect on Multi-Rotor wind turbine, making its findings preliminary at best. Additionally, the aerodynamic model used in [9, 14] does not account for the effect of tower and support structure on the aerodynamic loads. An aeroelastic model is presented for a Multi-Rotor wind turbine consisting of two rotors [16]. The paper concludes that the torsional stiffness of the tower for a Multi-Rotor system is more crucial than for a Single-Rotor case. The work is still ongoing and several improvement points are identified by the authors to modify the aeroelastic model of the Multi-Rotor wind turbine.

Although extensive research is underway with regards to CFD analysis Multi-Rotor wind turbines, there is still work to be done on the complete system design of Multi-Rotor systems. Accurate aeroelastic model of a Multi-Rotor wind turbine needs to be formulated in order to analyze the aeroelastic response of Multi-Rotor systems under turbulent wind and examine the resulting loads on Multi-Rotor wind turbine components [17]. Particularly, the loads on the tower and booms of a Multi-Rotor wind turbine needs to be quantified.

This paper presents an aeroelastic model of a Multi-Rotor wind turbine consisting of four rotors. The model is used to determine the aeroelastic response of the quad-rotor wind turbine under load cases selected from IEC-61400-1 [15] and compared to a single-rotor wind turbine with equal swept area. The standardization of components is one of the many advantages of Multi-Rotor wind turbines. One aspect of component standardization is the fact that all the currently existing blades are designed to generate aerodynamic torque that spin the rotors in the same direction. Therefore, this paper focuses on the analysis of co-rotating quad-rotor wind turbines, where all the rotors spin in the same direction.

II. Methodology

The quad-rotor wind turbine is modelled using the multi-body simulation (MBS) software SIMAPCK [18] coupled with the NREL aerodynamics software AerodynV15 [19] to calculate the aerodynamic blade loads. SIMPACK is an MBS software that employs both rigid and flexible elements to analyze nonlinear response of multi-body systems.

Figure 1a shows the SIMPACK model for the quad-rotor wind turbine. It consists of four WindPact 1.5MW clock wise spinning rotors [18]. The blades, booms, and the tower are modelled as flexible bodies, whose deformations are represented as elastic modes. The remaining wind turbine components (nacelle, hub, yaw-bearings, etc..) are modelled as rigid bodies. Figure 1b shows the structural layout and dimensions of the tower-boom assembly for the quad-rotor wind turbine. The tower is 136.75m long with four 36.75m long booms attached to the tower in Double-T configuration with the top and bottom booms separated by 73.5m. The tower is a hollow cylinder made of steel with Young's modulus of 2.1×10^{11} N/m^2 and mass density of 8100 kg/m^3. The bottom 70 % of the tower consists of a constant outer diameter of 4.3m and tapers linearly to 3.7m at the tower top. The elastic deformation of the tower is modelled using mode shapes corresponding to the first two Fore-Aft (FA) and Side-Side (SS) modes together with the first

torsion (TR) mode. The booms are 0.5(1 +δ_{sep})D long, where D is the rotor diameter and δ_{sep} is the minimum rotor separation distance, set to 5% of rotor diameter in the current model [6]. The booms are of the same material as the tower and are modelled as linearly tapered cylinders with the maximum diameter of 3.4m realized at the intersection between the booms and the tower (see Figure 1b) and a minimum diameter of 2.6m. Furthermore, an adapter at the boom tip is attached to support the rotor-nacelle assembly. The elastic deformation of the booms is modelled using linear combination of the boom's first Fore-Aft and Up-Down (UD) mode shapes together with the first torsion mode. The fore-aft and up-down mode shapes describe respectively the out-of-plane and in-plane deformation of the booms, with 'in-plane' defined as the plane containing the tower-boom assembly. The elastic deformation of the blades is modelled using linear combination of the first two flap modes and the first lag mode, with the blades assumed to be torsionally rigid. The foundation is modelled as clamped.

Additionally, a single-rotor wind turbine with a rated power of 6MW is modelled in SIMPACK to compare the response of the quad-rotor wind turbine to a single-rotor with equal swept area. The single-rotor wind turbine is a linearly scaled version of the NREL5MW Machine. The salient properties of both the quad-and single-rotor wind turbines are summarized in Table 1. The aerodynamic loads are calculated using AerodynV15, and these are passed to the wind turbine model in SIMPACK by means of the built-in interface module in SIMPACK. AerodynV15 uses Blade Element Momentum Theory (BEMT) to calculate the aerodynamic blades loads. It accounts for unsteady airfoil aerodynamics and includes skewed wake correction. However, it does not account for combination of tower-boom shadow on the axial wind velocity (normal to rotor disk). A correction model is formulated to take into account the effect of tower-boom shadow on the axial wind velocity.

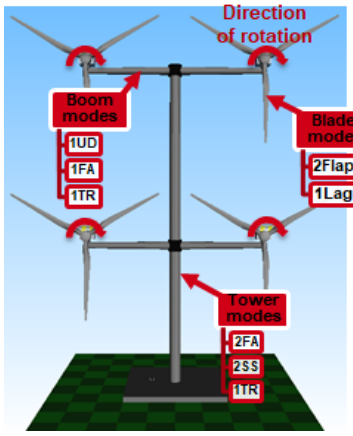

Fig. 1a: quad-rotor wind turbine model in SIMPACK.

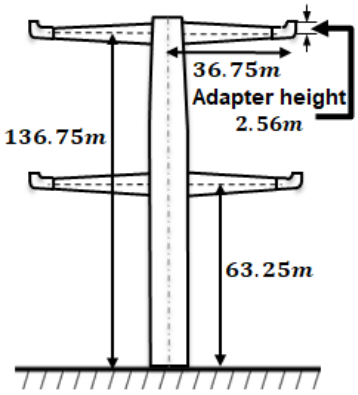

Fig. 1b: Dimensions of the Tower-Boom model.

Tab. 1: Gross Properties for Quad-and Single-Rotor wind turbine.

Parameters	Quad-Rotor	Single-Rotor
Rating(MW)	4×1.5	6
Control	Var Speed, Coll. Pitch	Var Speed, Coll. Pitch
Rotor, Hub Diameter(m)	70, 3.5	140, 7.0
Hub Height(m)	136.75(top) / 63.25(bottom)	100
Rated Wind Speed(m/s)	11.4	11.4
Rated Rotor Speed(rpm)	21.8	10.9
Rated Tip Speed(m/s)	80	80
Overhang(m), Shaft Tilt(deg), Precone(deg)	3.3, 0, 2.5	5.5, 0, 2.5

The axial velocity deficit of a tubular tower or boom is modelled using potential theory [20], with the correction to the axial incoming velocity given by:

$$\frac{u}{u_\infty} = \left(1 - \frac{0.25D^2(x^2-y^2)}{(x^2+y^2)^2}\right), \qquad (1)$$

where u_∞ is the undisturbed axial incoming velocity, D is the tower or boom diameter, x is the distance between the tower/boom to the rotor-plane, and y is the lateral distance from the flow axis of symmetry through the tower/boom center-line. Figure 2 shows an example of tower/boom correction of the axial incoming velocity, where the corrected velocity field (right most plot) is obtained by multiplying the pristine axial velocity filed (left most plot) with tower/boom velocity deficit field (center plot) calculated using equation 1. The velocity deficit field shows zero correction of the axial velocity (velocity deficit value of one) far away from the tower or boom while reduction in axial velocity is observed close to the disturbance source (tower or boom). This is a first order approximation for tower/boom shadow since the correction is applied at the start of the aeroelastic simulation; and therefore does not take into account the effect of boom and blade flexibility on the velocity deficit.

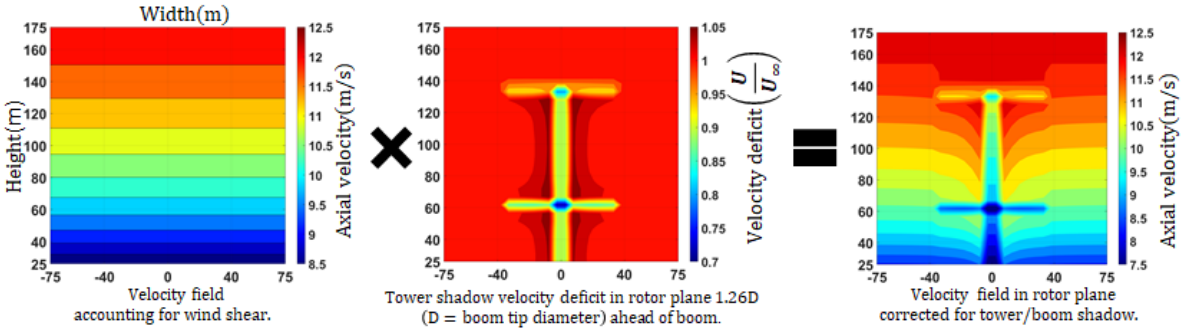

Fig. 2: Tower shadow correction on axial velocity.

Figure 3 shows the co-simulation strategy between Simpack coupled to Matlab Simulink. The Simpack module calculates the aeroelastic response of a wind turbine model and passes the rotor speed and the collective blade pitch angle, per rotor, to Simulink (denoted by the vector **y** in Figure 3). The controller module in Simulink calculates the generator torque and the collective blade pitch angle which is then passed to the Simpack model (denoted by the vector **u** in Figure 3). Since Simpack accepts only force and torque from Simulink, the collective blade pitch angle is converted to blade pitch torque by multiplying it with an effective pitch actuator (torsional) stiffness. The pitch actuator stiffness in Simpack is set to a large value to avoid pithing of the blades due to aerodynamic torque acting on the blades while allowing for the controller signal (collective blade pitch angle) to pitch the blades to the desired value.

The control strategy for the single- and quad-rotor wind turbine is to use a non-optimal (without a region 2.5) quadratic controller for the generator-torque below the rated speed while a collective pitch-to-feather PID controller is implemented above the rated speed; where the torque constant (generator-torque controller) and PID gains (blade pitch controller) are obtained or modified (in the case of the single-rotor wind turbine) from [20]. The control strategy does not account for non-power-production scenarios and does not include yaw control or generator speed filtering in the control loop.

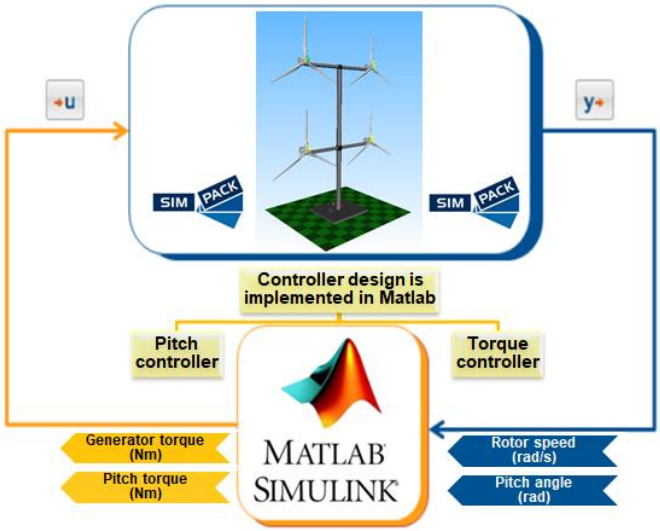

Fig. 3: Co-Simulation strategy to link Simpack model coupled with Simulink controller in Matlab (adapted from [18]).

III. Analysis cases

The performance of a quad-rotor wind turbine is analyzed considering three load cases from the International Electrotechnical Commision (IEC) 61400-1 [15]. An overview of the considered load cases from the IEC standard are listed in Table 2. These load cases cover nominal loads under normal wind profile, fatigue and ultimate loads under respectively normal and extreme turbulent wind. The remaining load cases from the IEC standard that cover parked condition, transportation, assembly, maintenance or repair are not considered. The safety factor on the loads is neglected, since it cancels out during a comparative study between single-and quad-rotor wind turbine.

Tab. 2: Considered load cases from IEC 61400-1 [13].

Design Load Case (DLC)	Wind type	Wind speed	Simulation time	Analysis
1.1 Power production	Normal wind speed profile	$U_{in} < U_h < U_{out}$	5min	Nominal
1.2 Power production	Normal turbulence model	$U_{in} < U_h < U_{out}$	4X10min	Fatigue
1.3 Power production	Extreme turbulence model	$U_{in} < U_h < U_{out}$	10min	Ultimate

U_h: hub-height wind speed, U_{in}: cut-in wind speed = 3m/s, U_{out}: cut-out wind speed = 25m/s

The open source software TurbSim [22] is employed to generate the incoming wind used to calculate the aerodynamic loads on wind turbine blades. TurbSim is a stochastic turbulence generation code producing a full-field flow that includes bursts of coherent turbulence with spatiotemporal consistency related to turbulent structures (eddies) in the flow. The normal wind speed profile is modelled using a power law with an exponent of 0.2 and the turbulent wind velocities are generated for a turbulence class of B and using the Von Karman turbulence model.

The present study compares the loads on the support structure of the quad-rotor and single-rotor turbine of equal machine rating. Figure 2 shows the monitored location, both on the quad-and single-rotor support structure. The monitored locations are highlighted using colored dots. The tower base loads on the single-rotor tower are compared with the quad-rotor tower base loads at the same location (shown by the red circles at the base of the towers). The yaw-bearings on the quad-rotor tower (shown with green and black circles in Figure 4) support the top and bottom booms and are attached to the tower in such a way to allow (asymmetric) yaw motion of the left and right rotors; with the yaw degree of freedom constrained in the present analysis. The loads on the tower top (shown with green circles on the single-rotor tower) are compared with the loads on the top and bottom yaw-bearings on the quad-rotor tower. Furthermore, the root loads and tip deflection of the booms are examined, where the boom root loads are indicated by the brown colored circles and the boom tip displacement are indicated by purple colored circles. Finally, the rotor power and thrust at the rotor nacelle(s) on both wind turbine configurations are examined (shown with the blue colored circles).

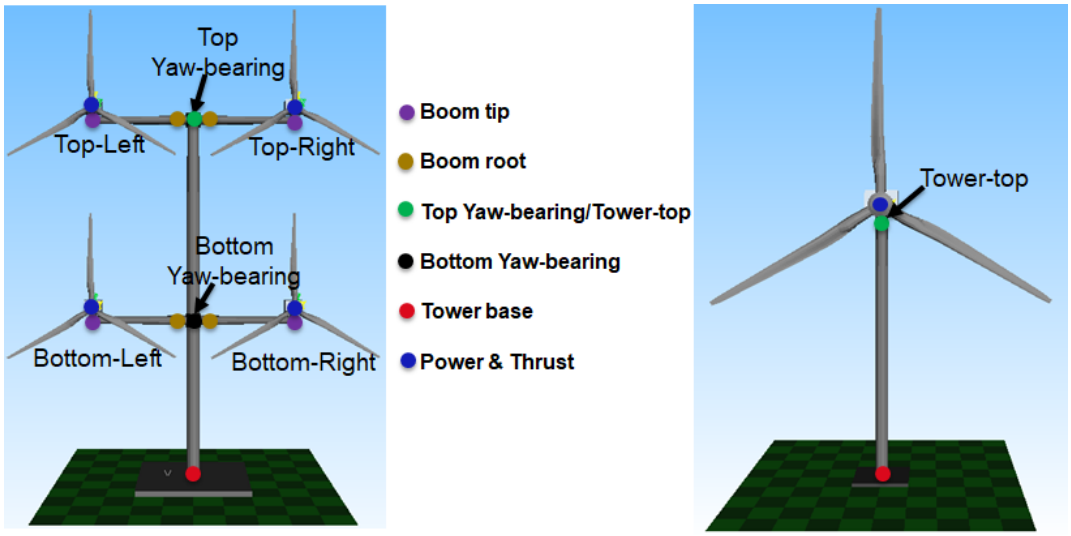

Fig. 4: Monitored locations shown with colored dots.

IV. Nominal Loads (IEC Load Case 1.1)

The first set of simulations is carried out for the load case covering power production under normal wind speed profile from the IEC standard shown in Table 2. A 5-minutes simulation is carried out for mean wind speed range between cut-in and cut-out, where the mean wind speed refers to the hub height wind speed on the single-rotor wind turbine.

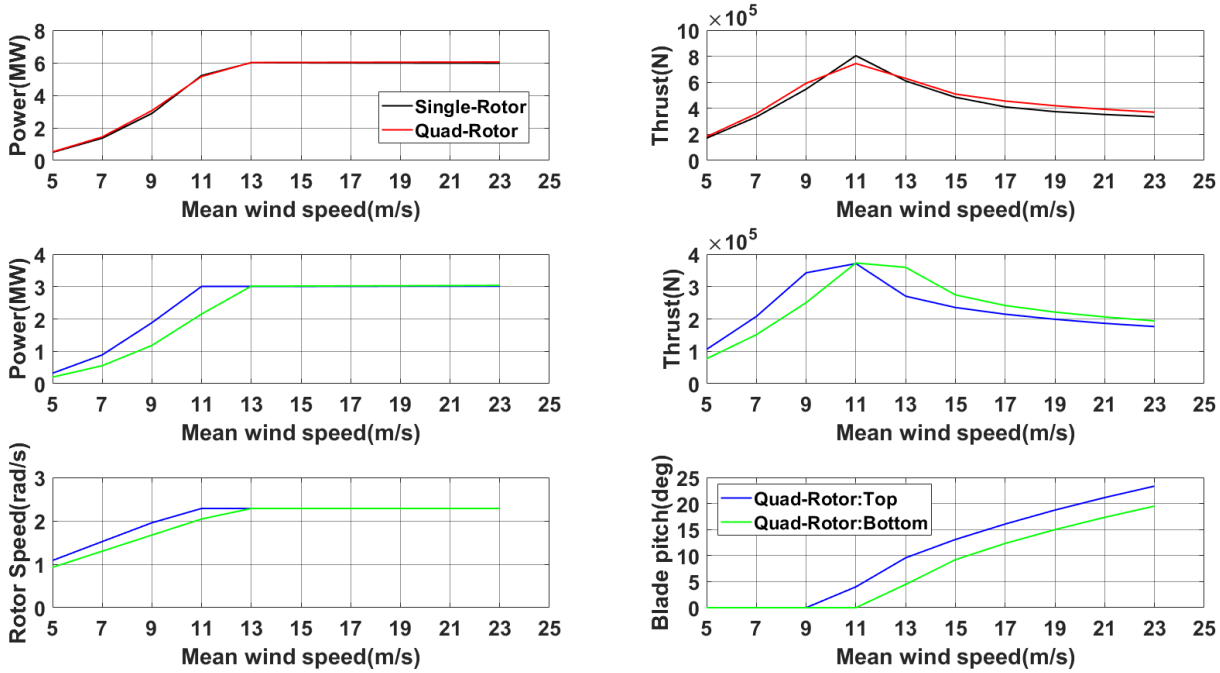

Fig. 5: Nominal power and thrust under steady wind for both wind turbine configurations.

Figure 5 presents power and thrust versus mean wind speed for the single-and quad-rotor wind turbines. Furthermore, the two center windows in Figure 5 show the power and thrust of the combined top and bottom rotors on the quad-rotor wind turbine, while the bottom two windows present the rotor speed and blade pitch angle. The power versus mean wind speed curve on the top left window shows that the quad-rotor configuration generates slightly higher power for below rated speeds (up to 6% at 9m/s). This can be attributed to the fact that the smaller rotors on the quad-rotor tower are able to operate more efficiently in the presence of wind shear, where the top rotors rotate faster due to higher wind speeds and the bottom rotors lower (see bottom left window). The effect of wind shear on power generation for the quad-rotor wind turbine is more evident on the center left window which shows that the top rotors achieve rated power for wind speed lower than the rated mean speed (at the hub height of the single-rotor wind turbine) and the bottom rotors achieve rated power at higher mean speed compared to the rated mean speed. This shows that the smaller rotors are able to optimize their rotational speed to the local wind speed condition and hence are more efficient in extracting power from the incoming wind, especially for below rated wind speeds (up to 6% more at 9m/s).

Furthermore, the top right window shows reduced peak thrust for the quad-rotor wind turbine but higher post rated thrust values when compared to the single-rotor wind turbine. The reduced peak thrust is the results of shifted thrust curve between the top and bottom rotors on the quad-rotor configuration caused by wind shear (see bottom right window in Figure 5). In the presence of wind shear, the top rotors achieve peak thrust at below rated wind mean wind speed while the bottom rotors at above rated wind speed. This causes the redistribution of the thrust value across the mean wind speed, resulting on one hand in reduction of the peak thrust while on the other, slightly higher thrust for post rated wind speeds. This is because the lower rotors are generating more thrust to produce same power at above rated mean speeds. For example, at 13m/s, both the top and bottom rotors produce the same power (3MW) but the bottom rotors generate more thrust because the blade pitch angle of the bottom rotors is lower than for the top rotors (see bottom right window in Figure 5).

The nominal root moment for the top and bottom booms together with boom tip deformation, under steady wind, is shown in Figure 6. The error bars in the figure indicate the peak-to-peak variation from the nominal value due periodic

loading by wind shear and tower/boom shadow. The left windows in Figure 6 show boom root moments while the right windows contain the boom tip deflection and twist. The Up-Down moment is caused by gravity load from rotor/nacelle mass resting at the boom tip and the vertical rotor shear force times their respective moment arm (boom length). The Up-Down moment is mainly dominated by the rotor/nacelle mass. The tip deflection associated with the Up-Down moment is the Up-Down displacement depicted in center right window, where the magnitude of the deflection is shown as a percentage of the boom length; showing similar trend as the Up-Down moment. Furthermore, larger peak-to-peak variation from nominal value is observed for increasing mean speed.

Figure 7 shows the displacement and velocity (in the direction of thrust) at the top of the single-rotor tower (shown with black line) together with top (shown in red) and bottom (shown in blue) yaw-bearings on the quad-rotor tower. Looking at Figure 7, the quad-rotor shows larger tower velocities than the single-rotor counterpart (particularly at the location of the top yaw-bearing) with increasing peak-to-peak variation in tower velocity for increasing mean wind speed. The increased tower velocity of the quad-rotor tower is the result of having a longer tower to support four rotors on a Double-T configuration; resulting in a more flexible tower with larger swing as compared to the single-rotor tower. Furthermore, higher 3p excitation frequency for the quad-rotor tower (which is double that of the single-rotor tower) also contributes to the increased quad-rotor tower velocity. The tower velocity, added to the variation in incoming wind due to wind shear and accounting for tower/boom shadow, further increases the peak-to-peak load variation across different components of the quad-rotor wind turbine.

Going back to Figure 6, the torsion moment on the boom root is the sum of rotor pitch moment, rotor mass times its overhang (see Table 1), and rotor thrust times the offset of the nacelle attachment from the boom axis (denoted as adapter height in Figure 1b). The torsion moment at the boom root is a function of the rotor thrust, evident by the fact that similar trend is observed between the two load components (see the thrust curve in Figure 5). Furthermore, the deviation from the mean value increases with increasing mean wind speed which is due to the additional tower velocity (see Figure 7). The trend in tip twist (bottom right window in Figure 6) is similar to the torsion moment at the boom root since, in both cases, the gravity load from the rotor mass, thrust, and rotor pitching moment are the driving loads. Decreasing magnitude in tip twist is observed for increasing mean wind speed, indicating that the torsion due to thrust plus rotor pitching moment (acting nose up) is opposite to the (static) torsion due to the mass of the rotor (acting nose down).

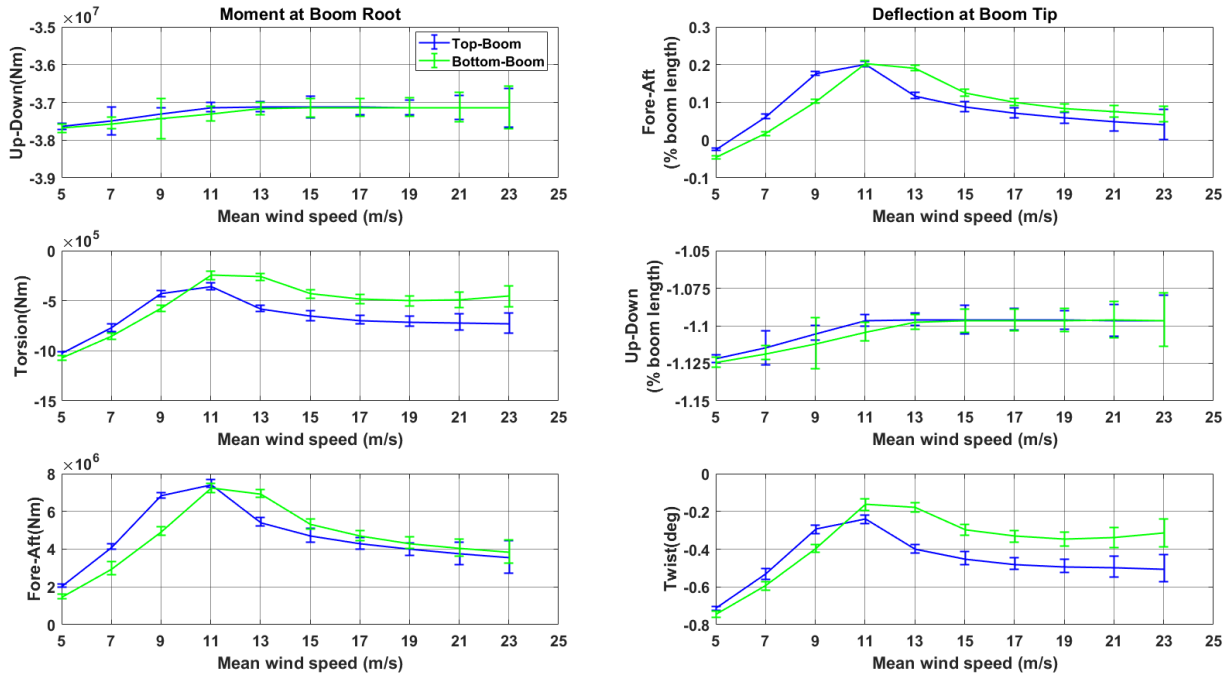

Fig. 6: Boom root moment and tip deflection under steady loads.

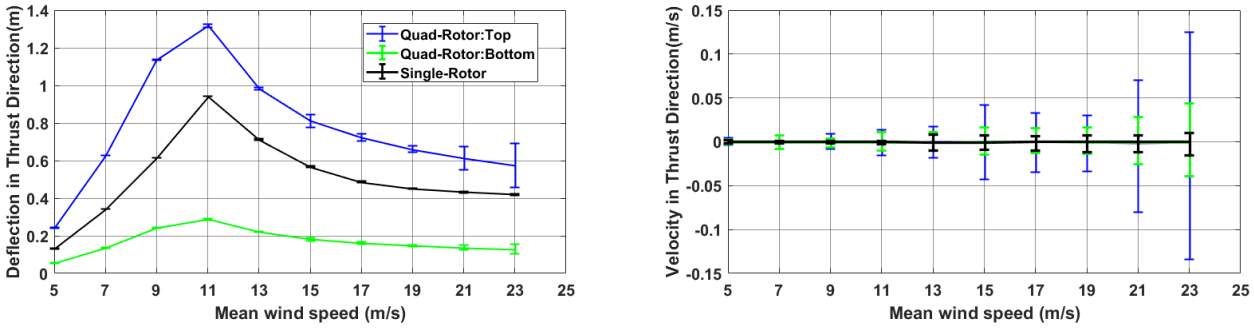

Fig. 7: Tower fore-aft displacement(left) and velocity (right) under steady wind.

Furthermore, the torsion and twist curves show that the bottom booms experience higher rotor pitching moment compared to the top booms; due to the bottom rotors encountering greater variation of wind speed over the rotor height as compared to the top rotors in the presence of wind shear with the bottom rotors experiencing the highest wind speed gradient. This results in a greater thrust differential between the top and bottom half of the rotor disk and thus increasing the pitching moment on the bottom rotors. Finally, the magnitude of tip twist is larger for the bottom booms for below rated wind speeds while the reverse is true for wind speeds above the rated wind speed, following the same trend as the rotor thrust versus mean wind speed curve shown in the bottom right window of Figure 5. A solution to minimize the peak-to-peak variation in boom tip twist (i.e. minimize oscillation in rotor pitching motion) would be to re-design the adapter by shortening the adapter-height (see Figure 1b).

The Fore-Aft moment at the boom root in Figure 6 has the same trend as the rotor thrust indicating this load component is the product of rotor thrust times the boom length; with the top booms experience higher loads for wind speeds below rated while the bottom booms see higher loads for above rated wind speeds. Furthermore, peak-to-peak variation in fore-aft moment increases for higher mean wind speeds, caused by increasing variation in tower velocity at higher wind speeds (see Figure 7).

The Fore-Aft displacement at the boom tip is also caused by the rotor thrust. While there is a larger variation in the fore-aft boom tip displacement (compared to the up-down tip deflection), the design driver in terms of boom stiffness is determined by the up-down boom tip displacement (which is orders of magnitude greater than fore-aft boom tip displacement). An alternative design for the booms to carry the same tip mass without drooping (large up-down boom tip deflection) could be to place the booms in a shallow V-shape configuration and attach a cable between the booms and the tower. This way, the cables will aid the booms in carrying the mass of the nacelle/rotor assembly, allowing for lighter boom design. Alternatively, internal I beam overlaid with thin cylindrical shell design could be implemented where the I beam is the load carrying component (carrying primarily the up-down bending loads due to the concentrated mass at the boom tip).

Figure 8 shows force and moment components at the tower top of the single-rotor turbine and at the top and bottom yaw-bearings of the quad-rotor turbine; with the force components shown in the left column of windows and the moment components in the right column. Looking at the shear force in the thrust direction, the single-rotor tower experiences higher loads than the yaw-bearing loads on the quad-rotor tower. The reduced rotor thrust that each yaw-bearing carries is due to reduced rotor area at the top and bottom rotors. The rotor thrust on each yaw-bearing is effectively reduced by half when compared to the rotor thrust on the single-rotor tower with larger rotor area; allowing for lighter design of yaw-bearings which reduces material cost. The peak shear force (in the direction of thrust) on the bottom yaw-bearing is shifted to the right compared to the peak force on the top yaw-bearing, mirroring the thrust curves in bottom left window of Figure 5, as expected.

On the single-tower, the nominal horizontal shear force along the boom axis (center left window in Figure 8) increases with increasing mean wind speed but with low peak-to-peak variation. Consequently, the nominal horizontal shear force on the quad-rotor tower (at the top and bottom yaw-bearings) does not (significantly) increase with mean speed but experiences larger increase (compared to single-rotor tower) in peak-to-peak variation (especially for post rated speeds). The increase in peak-to-peak load is due to the addition of the tower velocity to the incoming wind. Particularly, the top yaw-bearing sees larger peak-to-peak variation from the nominal horizontal shear force, reflecting

larger variation in velocity at the top of the quad-rotor tower (see Figure 7). Finally, the single-rotor tower experiences larger horizontal shear force (along the boom axis) compared to the yaw-bearings on the quad-rotor wind turbine, with similar reason as in the case of the shear force in the thrust direction.

The yaw-bearings on the quad-rotor tower experience reduced vertical force when compared to the single-rotor counterpart (see the bottom left window in Figure 8). This is advantageous in the design of yaw-bearings, since the bearings on a wind turbine need to support the weight of the nacelle/rotor assemble while facilitating the yaw-motion of the rotors. Reducing the normal loads on the bearings will increase their fatigue life or allows for a lighter design, reducing cost.

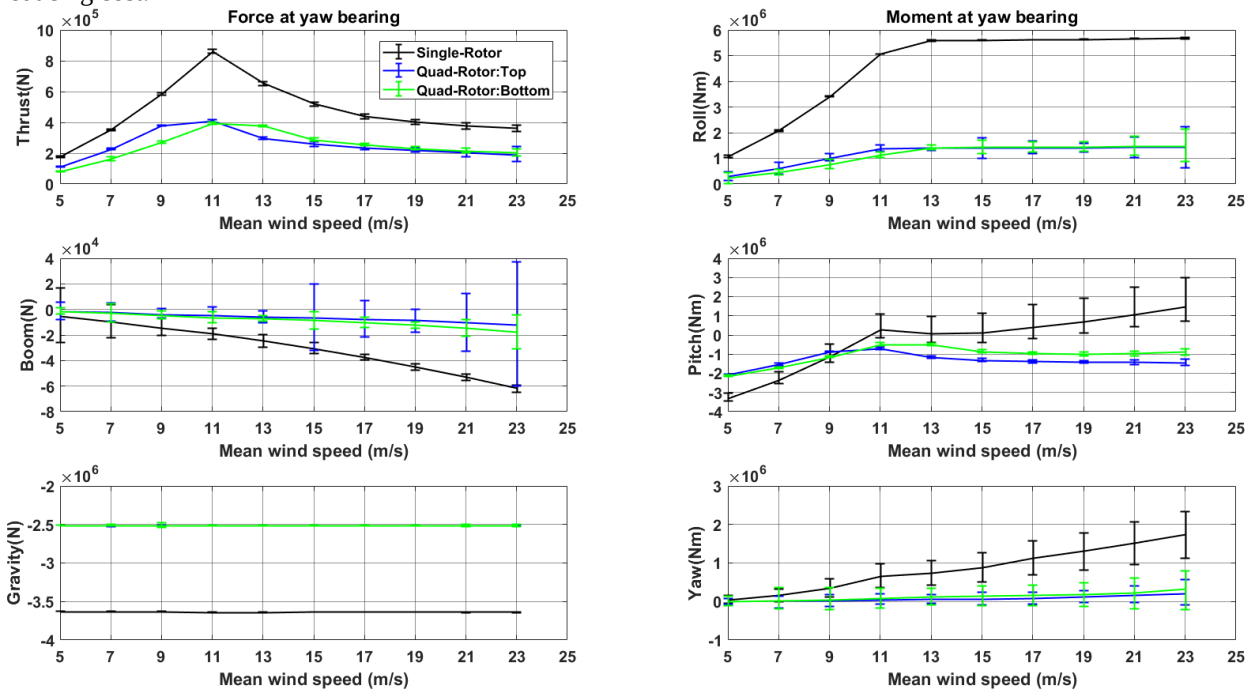

Fig. 8: Tower top force (left column) and moment (right column) under steady wind.

The top right window in Figure 8 shows the roll moment at the top of the single-rotor tower and at the top and bottom yaw-bearings on the quad-rotor tower. The roll moment on the yaw-bearings is lower than the roll moment at the top of the single-rotor tower, and the sum of the moments at the top and bottom yaw bearings on the quad-rotor are lower than the tower top moment for the single-rotor. This can be understood by examining the load components constituting the roll moment on the quad-rotor tower. Looking at Figures 1a and 1b, the roll moment at a yaw-bearing, in the case of co-rotating rotors, is the difference between the sum of the rotor roll moments on the left and right side of the tower and the moment caused by the in-plane horizontal rotor force times the adapter height. Under steady wind, roll moment due to in-plane vertical rotor force on the left and right rotors times the boom length cancels each other out at the yaw bearings. Since the roll moment caused by the in-plane horizontal rotor force acts opposite to the rotor roll moments, the overall roll moment on the quad-rotor tower is less than on the single-rotor.

The pitch moment at the top of the single-rotor tower (center right window in Figure 8) is in general larger in magnitude compared to the same load on the yaw-bearings for the quad-rotor turbine. Furthermore, the pitch moment on the single-rotor tower increases after the rated wind speed, while the pitching moment at the yaw bearings of the quad-rotor show much smaller variation with wind speed (especially beyond rated speed). Additionally, higher peak-to-peak value of pitch moment is observed at the top of the single-rotor tower compared to the same load on the yaw-bearings; since the larger rotor on the single-rotor tower sees larger variation in wind speed due to wind shear compared to the smaller rotors on the quad-rotor wind turbine.

Finally, the nominal yaw moment on the single-rotor tower and quad-rotor tower is shown in the bottom right window of Figure 8. As expected, the magnitude of the yaw moment at the top of the single-rotor tower is larger than on the top and bottom yaw-bearings of the quad-rotor turbine. Under steady wind, the thrust on the left and right rotors on

yaw-bearings cancel each other out leaving only the nominal rotor yaw moment on the smaller rotors. Furthermore, the mean and peak-to-peak yaw moment increases with increasing mean speed, with the single-rotor experiencing a larger increase in mean value compared to the yaw-bearings on the quad-rotor turbine.

The tower base forces and moments under steady wind are shown in Figure 9. The force components are presented in the left column windows while the moment components are shown in the right column windows. The shear force in thrust direction (also the tower base fore-aft moment) follows the same trend as the rotor thrust presented in Figure 5. This is to be expected since the shear force and the fore-aft moment at the tower base are driven by rotor thrust.

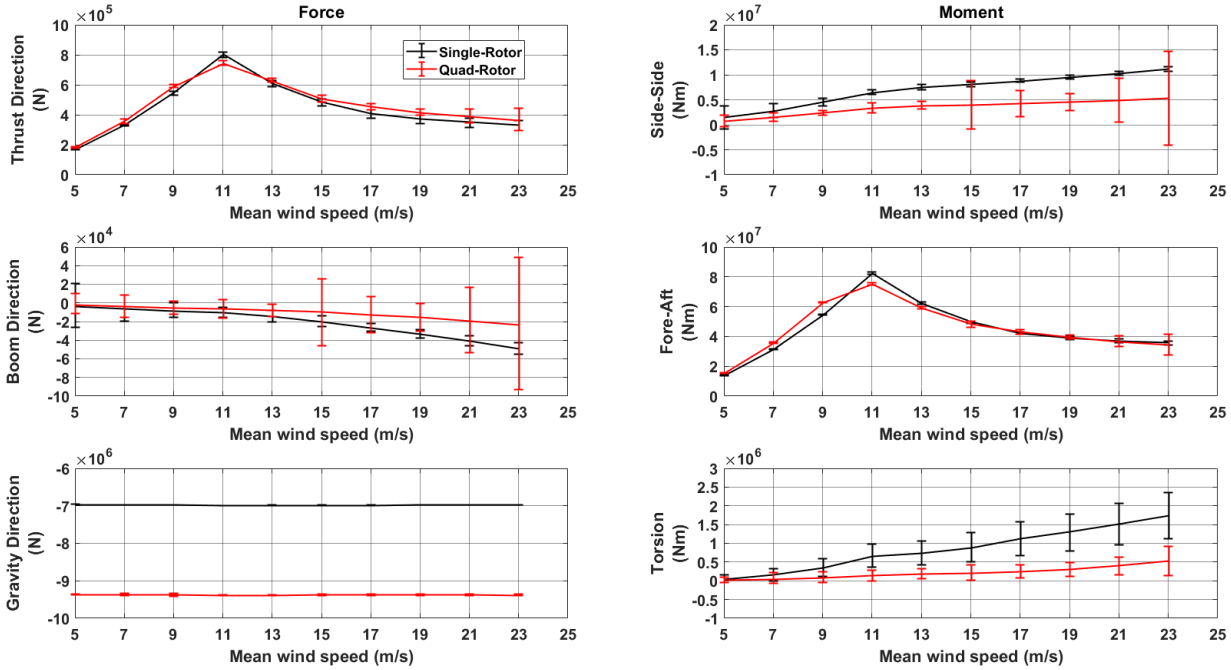

Fig. 9: Tower base force (left column) and moment (right column) under steady wind.

The center left window in Figure 9 shows the shear force along the boom axis (the tower root side-side force). The magnitude of the shear force, at the base of both towers, increases with increasing mean wind speed. Furthermore, for the quad-rotor tower, the peak-to-peak variation in the shear force increases with increasing mean wind speed, mirroring the case of the shear force at the tower top or yaw-bearings (see center left window in Figure 8). There is similarity in trend between the shear force (center left window in Figure 9) and the side-side moment (top right window in Figure 9), where the side-side moment is simply the shear force multiplied by the appropriate tower height value(s). Therefore, greater peak-to-peak variation in side-side moment is observed for quad-rotor tower compared to the single-rotor tower.

The normal force in the direction of gravity (see bottom left window in Figure 9) is larger on the quad-rotor tower than on the single-rotor tower. This is the results of the added mass of the four booms on the quad-rotor tower. As mentioned earlier, the design driver for the booms is the moment caused by the tip mass. Using cables to carry part of the concentrated tip mass allows for lighter boom design which in turn reduces the overall mass that the quad-rotor tower needs to carry.

Finally, the torsion moment at the base of the single-rotor tower is the same as the yaw moment at the tower top, while the torsional moment at the base of the quad-rotor tower is the sum of the yaw moment at the top and bottom yaw-bearings. Under steady wind condition, the nominal torsion at the tower base is smaller for the quad-rotor tower than for the single-rotor tower. This will not be the case under unsteady wind condition, where the left rotors see different incoming wind than the right rotors, causing differential thrust between left and right rotors that adds to the torsional moment at the base of a quad-rotor tower; which will be covered in the next section.

V. Fatigue Loads (IEC Load Case 1.2)

The next set of simulations covers fatigue assessment of the quad-rotor wind turbine. Particularly, the fatigue performance of the quad-rotor tower is compared with the fatigue response of a single-rotor tower. Four 10-minutes simulations are carried out at mean wind speeds between cut-in and cut-out in 2m/s increments covering power production under normal turbulent wind, where incoming turbulence in the simulations is generated with random seeds for good estimation of fatigue loads (see DLC 1.2 in Table 2). Life time Damage Equivalent Load (DEL) on the various wind turbine components is calculated using miners rule [23], with the lifetime DEL defined as:

$$\Delta S_{DEL} = \sqrt[m]{\frac{1}{u_o - u_i}\frac{1}{N_r}\int_{u_i}^{u_o}(f(u)\sum_{i=1}^{N}\Delta S_i^m n_i)du}, \qquad (2)$$

Where m is the inverse of the material wöhler slope, n_i is the number of load cycles at the stress amplitude ΔS_i^m, N_r is the reference number of cycles; u_o and u_i are respectively the cut-in and cut-out wind speeds. The wind speed probability distribution $f(u)$ is generated using a Weibull distribution with scale and shape parameters given respectively by 13 and 3. Furthermore, the present analysis includes (for both single-and quad-rotor turbines) pitch error of ±0.2 on blades 2 and 3 together with rotor mass imbalance due to additional mass of 2.3% (of the nominal blade mass) added to blade 1; to simulate deterioration of blade pitch actuator error during turbine's lifetime operation and error in blade manufacturing. Finally, the monitored locations in the present analysis consider only turbine components made of steel (see Figure 4). Therefore, a value of 4 [21] is used for the wöhler exponent m when calculating the damage equivalent load.

Fatigue performance of the quad-rotor wind turbine starts by comparing the normalized damage equivalent loads at the top and bottom yaw-bearings on the quad-rotor compared with the damage equivalent loads at the top of the single-rotor tower, as shown in Figure 10. The left and right windows in Figure 10 present respectively, the normalized damage equivalent force and moment, with the force DEL normalized by single-rotor tower top fore-aft shear force (in the direction of thrust) and the moment DEL normalized by the single-rotor tower top pitch moment. Damage equivalent fore-aft shear force on the quad-rotor yaw-bearings is less than the damage equivalent fore-aft shear force at the top of the single-rotor tower (by 23%-40%). The reduction is primarily due to lower thrust on the smaller rotors of the quad-rotor wind turbine. The top and bottom yaw-bearings carry smaller rotors, each supporting an equivalent rotor area half the size of the single-rotor wind turbine.

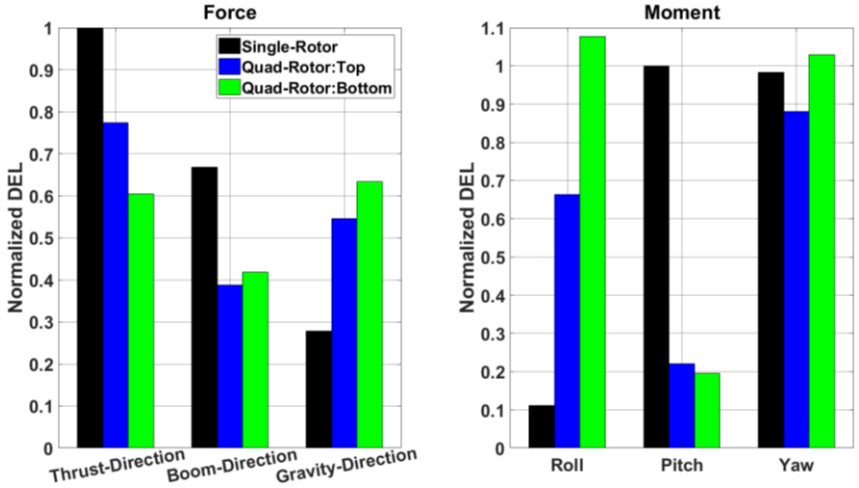

Fig. 10: Normalized DEL on the quad-rotor yaw bearings and at the top of the single-rotor tower. Force components are normalized by force in thrust-direction and moment components are normalized by pitch moment.

Reduced damage equivalent side-side shear force (along the boom axis) is observed on the quad-rotor turbine's yaw bearings (by 37%-42%), resulting from the smaller rotors carried by the yaw-bearings compared to the large rotor on the single rotor wind turbine. However, the normalized damage equivalent force in the direction of gravity at the quad-rotor turbine's yaw-bearings is higher compared to the single-rotor (by 96%-127%), with the bottom yaw-bearing experiencing slightly higher load than the upper bearing (due to larger wind shear gradient for the bottom rotors). Furthermore, the increase in DEL is attributed to boom inertia. Under unsteady wind, the acceleration of the booms (in the Up-Down direction) generates additional force that the yaw-bearings need to carry. Detailed evaluation of boom inertia vis-à-vis the roll-moment on the yaw-bearings is discussed next.

Figure 10 shows higher damage equivalent roll moment on the yaw-bearings compared to the same load at the top of the single-rotor tower (by 499%-870%). Figure 11a presents a schematic representation of the quad- and single-rotor tower together with the in-plane rotor forces and moments. Under unsteady wind condition, the vertical (F_z) and horizontal (F_y) in-plane rotor force are not identical between left and right rotors. These force components multiplied by their respective moment arm (boom length for F_z and adapter height for F_y) results in large roll moments at the yaw-bearing. This effect is shown in Figure 11b (QR and SR referring respectively to Quad- and Single-Rotor), where components of the damage equivalent roll moment on the bottom yaw-bearing are presented, with the in-plane forces contributing the highest to the DEL (84%), followed by boom inertia (13%) and with the smallest contribution coming from the rotor toque (3%). Between the vertical (F_z) and horizontal (F_y) in-plane rotor force, the highest contribution to the roll moment is from the vertical force since the moment arm of F_z (boom length) is at least an orders of magnitude larger than the moment arm of F_y (adapter height). Upon closer inspection of Figure 11b, the roll moment from the boom inertia alone is larger than the roll moment at the top of the single-rotor tower.

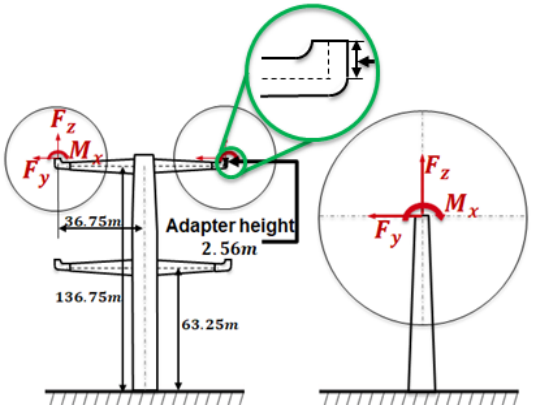

Fig.11a: Schematic representation of single-and quad-rotor support structure with in-plane rotor loads shown in red.

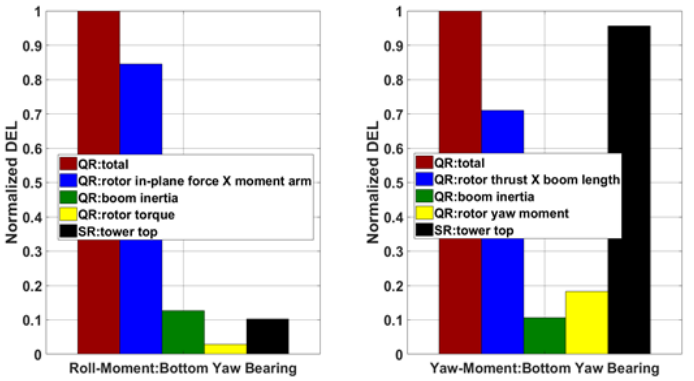

Fig.11b: Decomposition of Roll (left) and yaw (right) DEL moments in terms of the constituents together with DEL results for single-rotor tower.

Large reduction in damage equivalent pitch moment is observed for the yaw-bearings (78%-80%). This reduction is mainly attributed to reduced variation in incoming wind across the smaller rotors on the quad-rotor tower, where the effect of wind shear is significantly smaller than on the single-rotor wind turbine. Presence of booms on the quad-rotor tower does not have influence on the pitch moment by amplifying the rotor forces in a similar fashion to the roll and yaw moments. Considering the resultant in-plane moment (vector sum of roll and pitch) at the quad-rotor turbine's yaw-bearings, 9% increase in DEL is observed for the bottom yaw-bearing and 30% reduction for the top yaw-bearing compared to the resultant moment at the top of the single-rotor tower. Furthermore, Figure 11b shows the dominant components of the damage equivalent yaw moment on the bottom yaw-bearing together with the yaw moment DEL at the top of the single-rotor tower. In the case of the yaw moment, the highest contribution is from the rotor thrust (which is not identical between left and right rotors under unsteady wind) times the boom length (71%), followed by rotor's yaw moments (18%), with the lowest contribution coming from the boom inertia (11%). Going back to Figure 10, the damage equivalent yaw moment on the yaw-bearings is of the same order of magnitude to that of the single rotor (-10% to +5%).

Figure 12 shows the normalized damage equivalent force (left) and moment (right) values at the base of the single- and quad-rotor tower. The force and moment DEL are normalized respectively by the single-rotor tower root shear force (in thrust direction) and fore-aft moment at the base of the single-rotor tower.

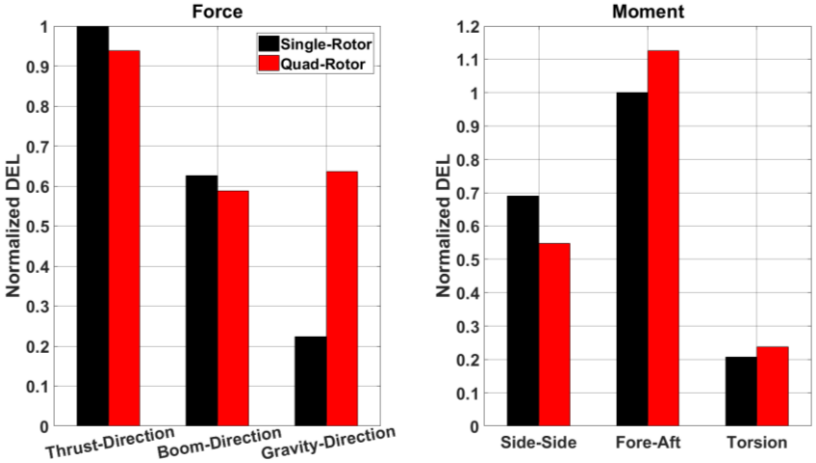

Fig. 12: Normalized DEL at the base of the single-and quad-rotor tower. Force components are normalized by single-rotor tower base shear force (in thrust direction) and moment components are normalized by fore-aft moment.

The fore-aft tower root shear force (in thrust direction) is comparable between the single- and quad rotor tower 6% lower on quad-rotor tower). The side-side tower root shear force (along the boom axis) is also comparable between the two tower configurations (6% lower on quad-rotor tower). On the other hand, the tower root normal force (in the direction of gravity) is 184% higher on the quad-rotor tower. This increase in DEL is the contribution of boom inertia similar to the case of DEL load on the yaw-bearings (see Figure 11).

A small difference in damage equivalent moment (at the tower base) is observed between the single- and quad-rotor turbine; with the quad-rotor tower experiencing 21% reduction in side-side moment, 13% increase in fore-aft moment, and 15% increase in torsion moment compared to the single-rotor tower.

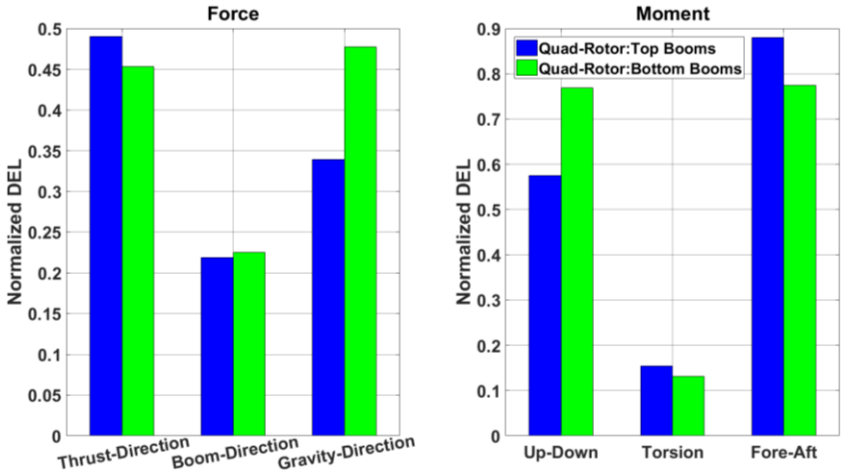

Fig. 13: Normalized DEL at boom root. force components are normalized by the DEL of the single-rotor tower top shear force (in thrust direction), moment are normalized by the pitch DEL at the single-rotor tower top.

Figure 13 presents the normalized damage equivalent force (left) and moment (right) results at the top and bottom booms attached to the quad-rotor tower. Damage equivalent force components are normalized by the DEL of the single-rotor tower top shear force (in thrust direction), whereas components of the damage equivalent moment are normalized by the damage equivalent pitch moment at the single-rotor tower top. The damage equivalent boom root

shear forces in the fore-aft (thrust) direction and axial direction (along the boom length) are similar between the top and bottom booms. On the other hand, the boom root vertical shear force (in the direction of gravity) is higher on the bottom booms (by 41%). This large increase in DEL on the bottom booms is largely due to the larger wind gradient caused by wind shear on the lower rotors. Overall, the net damage equivalent force at the boom root is half of the damage equivalent load at the top of the single-rotor tower, with the design driver being the shear force in the direction of thrust.

The bottom booms experience higher up-down damage equivalent moment, by 34%, while the torsion DEL is similar between the top and bottom booms. Large Up-Down damage equivalent moment at the boom root is caused primarily by the in-plane vertical rotor force (F_z) and the boom inertial load, mirroring the larger vertical damage equivalent shear force at the root of the bottom booms (compared to the top booms). Finally, the Fore-Aft damage equivalent moment is 14% higher on the top booms, similar to the force-aft damage equivalent shear force at root of the booms.

VI. Ultimate Loads (IEC Load Case 1.3)

The final set of results cover comparison of the quad-rotor wind turbine response under extreme turbulent wind to the single-rotor with equal machine rating. Simulations are carried out for the load case covering power production under extreme turbulence (see table 2). A 10-minutes simulation is carried out for the (single-rotor) mean hub-height wind speed ranging between cut-in and cut-out. Furthermore, the analysis includes (for both single- and quad-rotor turbines) pitch error of ±0.2 on blades 2 and 3 together with blade mass imbalance, with additional mass of 2.3% (of the nominal blade mass) added to blade 1. Ultimate loads on the various components is determined by extracting the minimum and maximum values from the load time history.

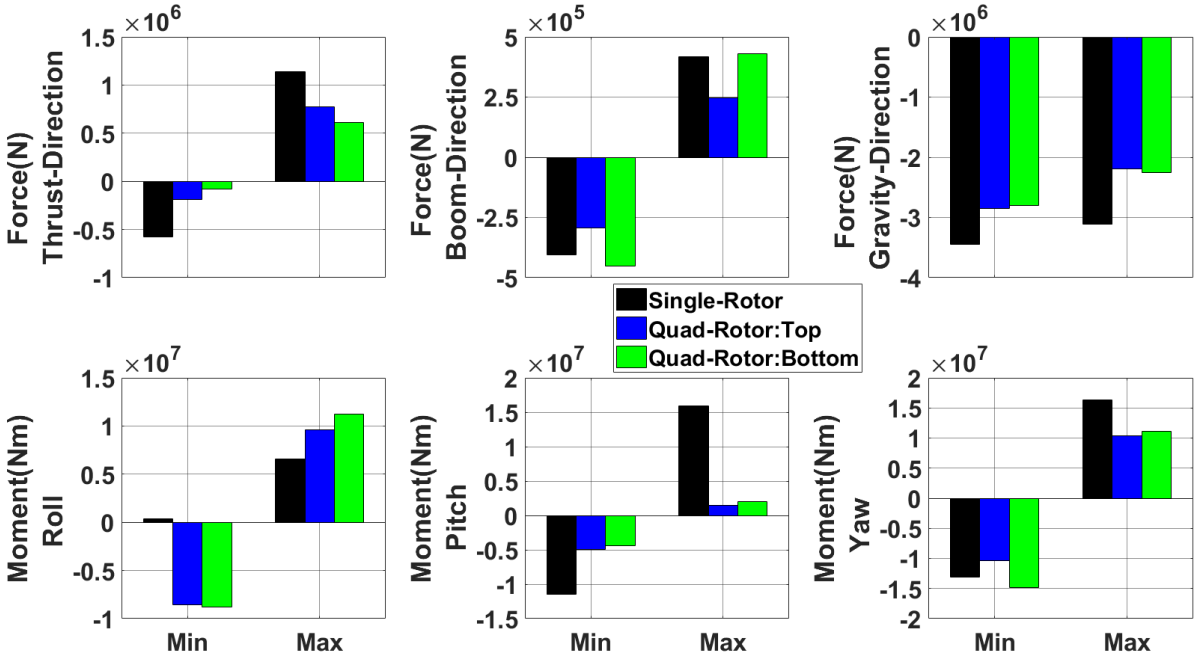

Fig. 14: Ultimate loads at the top and bottom yaw bearings on quad-rotor tower, compared to the loads at the top of the single-rotor tower.

Figure 14 presents the ultimate loads at the top and bottom yaw-bearings of the quad-rotor tower together with the ultimate loads at the top of the single-rotor tower. The top row of windows shows the minimum and maximum value of the force components while the bottom row of windows shows the minimum and maximum value of the moment components. The ultimate fore-aft shear force (in the direction of thrust, see top left window) is lower on the yaw-bearings of the quad-rotor turbine compared to the fore-aft shear force at the top of the single-rotor tower (32% for the top and 47% for the bottom). Furthermore, the negative shear force (in the direction of thrust), particularly on the

single-rotor tower top, is attributed to the interaction between the inertial and aerodynamic forces; this is explained using Figure 15, where a four minutes long time history of key responses at the top of the single-rotor tower are presented.

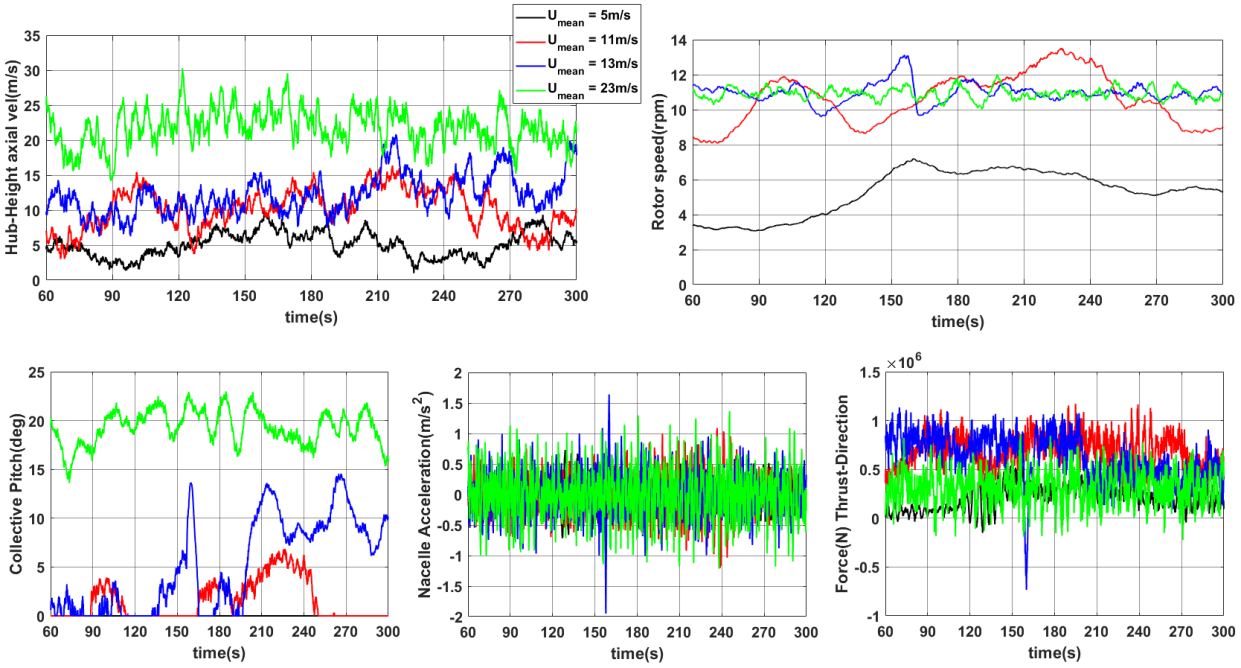

Fig. 15: A four-minute time history of key responses at the top of the single-rotor tower, each color representing response at different hub-height mean wind speed.

The top left and right window in Figure 15 show respectively four hub-height axial wind speed and the corresponding rotor speed. The bottom left window presents the collective pitch angle, the bottom center window shows the translational acceleration (in thrust direction) of the nacelle/hub assembly, and the bottom right window shows the resulting shear force (in thrust direction) at the top of the single-rotor tower. Looking at Figure 15, large negative shear force is seen for hub-height mean wind speed just above the rated value (for hub-height axial velocity of 13m/s, blue curve); showing that combination between sudden increase in collective pitch angle accompanied by a negative acceleration of the concentrated mass can result in large negative shear force in the direction of thrust. For example, looking at the time history for the hub-height wind speed of 13m/s (blue curve) around 150 seconds into the simulation, the incoming wind increases rapidly from below rated wind speed to above rated wind speed (roughly from 8m/s to 15m/s); this is accompanied by a jump in rotor speed (top right window), with the pitch controller attempting to reduce the sudden increase of the rotor speed (above the rated value) by increasing the collective blade pitch angle (bottom left window). The increase in collective blade pitch angle lowers the blade lift resulting in sudden reduction of rotor thrust followed by negative acceleration of the nacelle/rotor assembly (bottom center window). Finally, the difference between the reduced aerodynamic load (rotor thrust) and the negative inertial force results in negative vertical shear force at the tower top (bottom right window). The interaction between rotor aerodynamic load and rotor/nacelle inertia increases for increasing rotor area and overall mass at the tower top. Therefore, the (combined) negative shear force (in thrust direction) on the yaw-bearings of the quad-rotor tower is smaller than the negative shear force at the top of the single-rotor tower.

Going back to Figure 14, magnitude of the side-side shear force (along the boom axis, see top center window) is lower on the top yaw-bearings (by 33%) while it is higher on the bottom yaw-bearings (by 8%) compared to the same force at the top of the single-rotor tower. Furthermore, the normal force, in the direction of gravity, is lower on the top and bottom yaw-bearings of the quad-rotor tower (highest reduction of 19% for the bottom yaw-bearing) compared to the same force on the single-rotor tower; a consequence of smaller rotors that the yaw bearings need to carry compared to the larger rotor and nacelle on the single-rotor tower. Low normal load is advantageous in the design of bearings that go into the actuator that rotates (yaws) wind turbine rotors into the incoming wind.

The ultimate roll moment (bottom left window in Figure 14) is higher on the quad-rotor tower compared to the single-rotor tower top, with 42% and 75% increase at the top and bottom yaw-bearings respectively. This large increase in roll moment on the yaw-bearings is due to the additional roll moment coming from the in-plane rotor vertical force multiplied by the boom length (see Figure 11a and 11b). Under unsteady wind condition, the moment contribution from the in-plane vertical shear force between the left and right rotors do not cancel each another out. This has been extensively elaborated in the previous (IEC Load Case 1.2) section. Conversely, the ultimate pitch moment on the yaw-bearings is lower at least by 72% (opposite in sign) compared to the ultimate pitch moment at the top of the single-rotor tower. The significant reduction in pitch moment on the yaw-bearings (even when added together) is from lower variation of incoming wind (due to wind shear) over the smaller rotors compared to the larger rotor on the single-rotor tower. Considering the resultant in-plane moment (vector sum of roll and pitch) at the quad-rotor turbine's yaw-bearings, a reduction in ultimate load of 37% (at the top) and 30% (at the bottom) is observed compared to the resultant load at the single-rotor tower top. Finally, magnitude of the ultimate yaw moment at the top yaw-bearing is 29% smaller than at the single-rotor tower top, while the difference is negligible for the bottom yaw-bearing on the quad-rotor tower.

Next, Figure 16 presents the ultimate load at the base of the single- and quad-rotor towers subjected to unsteady wind. The top three windows show force components while the bottom three windows show moment components. The ultimate fore-aft shear force (in the direction of thrust, see top left window) is similar between the quad-and single-rotor tower. The ultimate side-side shear force (along the boom axis) at the tower base is 31% larger on the quad-rotor tower compared to the single-rotor tower. Furthermore, the normal force (in the direction of gravity) is 46% higher on the quad-rotor tower, due to additional mass of the booms that support the four rotors.

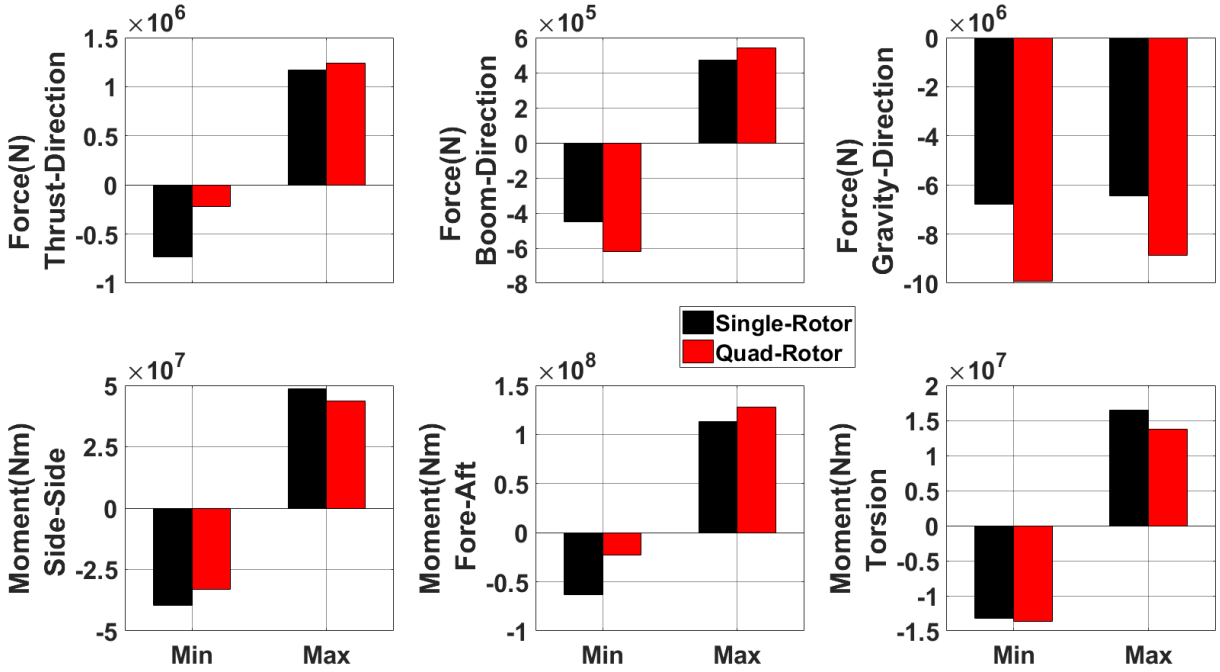

Fig. 16: Ultimate loads at the base of the single- and quad-rotor tower.

The ultimate side-side moment (bottom left window) on the quad-rotor tower is 10% lower than on the single-rotor tower. The ultimate fore-aft moment at the base of the quad-rotor tower is 15% higher than on the single-rotor tower. Although in the case of steady wind, the total rotor thrust on the quad-rotor wind turbine is comparable to the thrust on the single-rotor counterpart (see Figure 5), combination of unsteady wind with increased flexibility of the quad-rotor tower increases the unsteady thrust on the quad-rotor tower resulting in higher fore-aft moment at the tower base. The ultimate torsion value at the base of the quad-rotor tower is lower by 16% compared to the torsion at the base of the single-rotor tower.

Finally, Figure 17 presents the ultimate load at the boom roots together with extreme deformation and rotation of boom tip subjected to unsteady wind. The top row of windows in Figure 17 show the root moments while the bottom row of windows show the tip deflection and rotation, with the tip deflections presented as a percentage of the boom length. The booms experience large Up-Down moment causing large Up-Down boom tip displacement (bottom center window in Figure 17).

Furthermore, large peak-to-peak tip twist of up to 3deg is observed (bottom right window), with the tip twist heavily skewed to the nose down (negative) direction; suggesting that the rotor mass is the main contributor to large negative torsional moment on the booms (see top center window in Figure 17). The design option to minimize the peak-to-peak variation in boom tip twist is to increase the torsional stiffness of the booms or to reduce the torsional moment on the booms (or a combination of both). The peak-to-peak variation in torsional moment could be reduced by redesigning the adapter (interface between the booms and the rotor/nacelle assembly, see Figure 11a) such that the distance between the rotor hub and the boom axis is minimized. This will reduce the contribution of the rotor thrust to the boom torsion. Finally, the top booms experience higher fore-aft moment than the bottom booms (see top right window in Figure 17), which is the result of higher mean wind speed at the top rotors than on the bottom rotor due to wind shear. This in turn results in larger fore-aft tip deflection of the top booms (bottom left window).

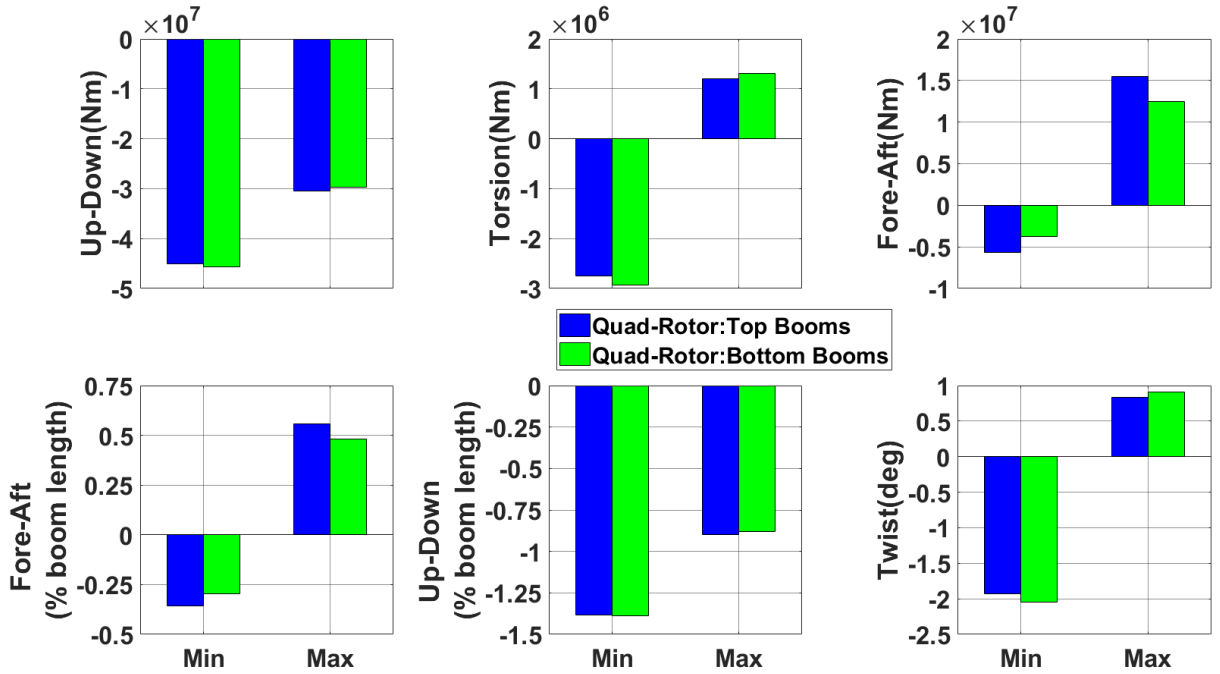

Fig. 17: Ultimate loads at the boom root together with extreme deformation and rotation of boom tip under unsteady wind.

Conclusion

A quad-rotor wind turbine with combined rated power of 6MW and a single-rotor with equivalent machine rating are modelled in SIMAPCK coupled with AerodynV15 (including turbulent wind input from TurbSim) to calculate the aerodynamic loads on the rotors. A correction for tower/boom shadow is implemented in Matlab to account for reduction in (axial) incoming wind due to the presence of support structures that carry the rotors. The performance of the quad-rotor wind turbine, with the single-rotor as baseline, is carried out for load cases selected from wind turbine certification standard (IEC-61400-1) covering: nominal loads under normal wind speed profile, fatigue loads under normal turbulence, and ultimate loads under extreme turbulence; with the following key takeaways:

- Under normal wind profile, the quad-rotor wind turbine generates up to 6% higher nominal power below the rated wind speed (at the hub-height of the single-rotor wind turbine). This is attributed to the fact that the smaller rotors on the quad-rotor tower are able to operate more efficiently in the presence of wind shear, where the top rotors are rotating slightly faster due to higher wind speed and the bottom rotors slightly lower.

- An examination of the quad-rotor boom (support the individual rotors and attach to the main tower) root loads and boom tip deflections indicates that gravitational effects dominate resulting in large up-down boom root bending moment and boom tip vertical displacement. Under turbulent wind, the boom tip experiences large peak-to-peak twist variation (in the order of 3 deg). This suggest that design modifications are necessary to carry gravitational loads (for example use of supporting cables) and increase of boom torsional stiffness may be required.
- Comparing the damage equivalent loads (DEL) under normal turbulence at the quad-rotor yaw bearings to the tower-top DEL at the single-rotor yaw bearing, the fore-aft and side-side loads are significantly lower while the normal load is around a factor of 2 higher for the quad-rotor turbine. The roll moments are 5-9 times higher due to imbalance in the vertical rotor hub forces on the quad-rotor turbine, but the pitching moment is 80% lower than the large single-rotor turbine would experience at the yaw-bearing. Considering combined in-plane moment (vector sum of pitch and roll moment), the DEL at the top yaw-bearing is 30% lower and 9% higher at the bottom yaw-bearing compared to the in-plane moment resultant at the single-rotor yaw-bearing.
- Under extreme turbulence, comparing the quad-rotor tower root loads to those of the single-rotor turbine, the side-side force is up to 31% higher, the force-aft bending moment is up to 15% higher, and the normal force is up to 46% higher due to additional boom/nacelle inertial loads.

Acknowledgments

This study was funded by the New York State Energy Research and Development Authority (NYSERDA) and General Electric (GE) Renewables under Award No.127346, Quad-Rotor Wind Turbine, with Mr. Scott Larsen (NYSERDA), Mr. Peter Maxwell (GE) as the Program Managers. Their support is gratefully acknowledged. NYSERDA and GE have not reviewed the information contained herein, and the opinions expressed in this report do not necessarily reflect those of NYSERDA or GE.

References

[1] Holst, H., "Opfindelsernes Bog,Nordisk Forlag," 1923.

[2] Honnef, H., "Windkraftwerke, Vieweg," 1932.

[3] Jamieson, P., and Hassan, G., *Innovation in wind turbine design*, Vol. 2, Wiley Online Library, 2011.

[4] Smulders PT., Orbos S., Moes C., "Aerodynamic Interaction between Two Wind Rotors set next to each other in One Plane." EWEC, Hamburg, 1984.

[5] Jamieson, P., and Branney, M., "Multi-rotors; a solution to 20 MW and beyond?" *Energy Procedia*, Vol. 24, 2012, pp. 52–59.

[6] van der Laan, P., Andersen, S. J., García, N. R., Angelou, N., Pirrung, G., Ott, S., Sjöholm, M., Sørensen, K. H., Neto, J. X. V., Kelly, M. C., et al., "Power curve and wake analyses of the Vestas multi-rotor demonstrator," *Wind Energy Science*, Vol. 4, No. 2, 2019, pp. 251–271.

[7] Chasapogiannis, P., Prospathopoulos, J. M., Voutsinas, S. G., and Chaviaropoulos, T. K., "Analysis of the aerodynamic performance of the multi-rotor concept," *Journal of Physics: Conference Series*, Vol. 524, IOP Publishing, 2014, p. 012084.

[8] van der Laan, M. P., and Abkar, M., "Improved energy production of multi-rotor wind farms," *Journal of Physics: Conference Series*, Vol. 1256, IOP Publishing, 2019, p. 012011.

[9] Jamieson, P., Chaviaropoulos, T., Voutsinas, S., Branney, M., Sieros, G., and Chasapogiannis, P., "The structural design and preliminary aerodynamic evaluation of a multi-rotor system as a solution for offshore systems of 20 MW or more unit capacity," *J Phys Conf Ser*, Vol. 5241, 2014, p. 012084.

[10] Ghaisas, N. S., Ghate, A. S., and Lele, S. K., "Large-eddy simulation study of multi-rotor wind turbines," *Journal of Physics: Conference Series*, Vol. 1037, IOP Publishing, 2018, p. 072021.

[11] Ghaisas, N. S., Ghate, A. S., and Lele, S. K., “Effect of tip spacing, thrust coefficient and turbine spacing inmulti-rotor wind turbines and farms,” *Wind Energy Science Discussions*, Vol. 2019, 2019, pp. 1–28. doi:10.5194/wes-2019-31, URL https://www.wind-energ-sci-discuss.net/wes-2019-31/.

[12] Bastankhah, M., and Abkar, M., “Multirotor wind turbine wakes,” *Physics of Fluids*, Vol. 31, No. 8, 2019, p. 085106. doi:10.1063/1.5097285, URL https://doi.org/10.1063/1.5097285.

[13] Ulhas, H., Jitesh, D., Gandhi, F., Onkar, S., “Analysis of Interactional Aerodynamics in Multi-Rotor Wind Turbines using Large Eddy Simulations,” *AIAA Scitech 2020 Forum, 2020, p. 1489*

[14] Jamieson, P., and Branney, M., “Structural considerations of a 20mw multi-rotor wind energy system,” *Journal of Physics: Conference Series*, Vol. 555, IOP Publishing, 2014, p. 012013.

[15] “IEC 61400-12-1 Ed. 1: Wind turbines – Part 12-1: Power performance measurements of electricity producing wind turbines, International Electrotechnical Commission,” 2005.

[16] Ismaiel, A., and Yoshida, S., “Aeroelastic Analysis of a Coplanar Twin-Rotor Wind Turbine,” *Energies*, Vol. 12, No. 10, 2019, p. 1881.

[17] Watson, S., Moro, A., Reis, V., Baniotopoulos, C., Barth, S., Bartoli, G., Bauer, F., Boelman, E., Bosse, D., Cherubini, A., et al., “Future emerging technologies in the wind power sector: A European perspective,” *Renewable and Sustainable Energy Reviews*, Vol. 113, 2019, p. 109270.

[18] Rulka, W., “SIMPACK—A computer program for simulation of large-motion multibody systems,” *Multibody Systems Handbook*, Springer, 1990, pp. 265–284.

[19] Jonkman, J., Hayman, G., Jonkman, B., Damiani, R., and Murray, R., “AeroDyn v15 User’s Guide and Theory Manual,” *NREL: Golden, CO, USA*, 2015.

[20] Dykes, K. L., and Rinker, J., “WindPACT Reference Wind Turbines,” Tech. rep., National Renewable Energy Lab.(NREL), Golden, CO (United States), 2018.

[21] Sharpe, D., and Sharpe, D., *Wind Energy Handbook*, John Wiley & Sons, Ltd, 2001.

[22] Jonkman B. J. and Kelly N.D., "Overview of the TurbSim Stochastic Inflow Turbulence Simulator," *Technical Report*, National Renewable Energy Lab.(NREL), Golden, CO (United States), 2006

[23] Pérez-Campuzano, Darío and Gómez de las Heras-Carbonell, Enrique and Gallego-Castillo, Cristóbal and Cuerva, Alvaro, "Modelling damage equivalent loads in wind turbines from general operational signals: Exploration of relevant input selection methods using aeroelastic simulations," *Wind Energy Journal*, Vol. 21, No. 6, 2018, pp. 441–459.